IOP Publishing New J. Phys. 18 (2016) 103048 doi:10.1088/1367-2630/18/10/103048

New Journal of Physics
The open access journal at the forefront of physics

Deutsche Physikalische Gesellschaft DPG
IOP Institute of Physics

Published in partnership with: Deutsche Physikalische Gesellschaft and the Institute of Physics

OPEN ACCESS

RECEIVED
28 June 2016

REVISED
29 August 2016

ACCEPTED FOR PUBLICATION
26 September 2016

PUBLISHED
25 October 2016

PAPER

Interface propagation in fiber bundles: local, mean-field and intermediate range-dependent statistics

Soumyajyoti Biswas[1,3] **and Lucas Goehring**[1,2]

[1] Max Planck Institute for Dynamics and Self-Organization, Am Fassberg 17, D-37077 Göttingen, Germany
[2] School of Science and Technology, Nottingham Trent University, Clifton Lane, Nottingham, NG11 8NS, UK
[3] Author to whom any correspondence should be addressed.

E-mail: soumyajyoti.biswas@ds.mpg.de **and** lucas.goehring@ntu.ac.uk

Keywords: fiber bundle model, interface, avalanche statistics, fracture, roughness

Abstract

The fiber bundle model is essentially an array of elements that break when sufficient load is applied on them. With a local loading mechanism, this can serve as a model for a one-dimensional interface separating the broken and unbroken parts of a solid in mode-I fracture. The interface can propagate through the system depending on the loading rate and disorder present in the failure thresholds of the fibers. In the presence of a quasi-static drive, the intermittent dynamics of the interface mimic front propagation in disordered media. Such situations appear in diverse physical systems such as mode-I crack propagation, domain wall dynamics in magnets, charge density waves, contact lines in wetting etc. We study the effect of the range of interaction, i.e. the neighborhood of the interface affected following a local perturbation, on the statistics of the intermittent dynamics of the front. There exists a crossover from local to global behavior as the range of interaction grows and a continuously varying 'universality' in the intermediate range. This means that the interaction range is a relevant parameter of any resulting physics. This is particularly relevant in view of the fact that there is a scatter in the experimental observations of the exponents, in even idealized experiments on fracture fronts, and also a possibility in changing the interaction range in real samples.

1. Introduction

The fiber bundle model, introduced in [1], is a useful approach for modeling catastrophic failures in disordered solids from a microscopic point of view [2, 3]. It aims at using the minimal ingredients that nonetheless capture the universal statistical features associated with phenomena [4–6] such as: the breaking of disordered samples like wood [7], glass [8], polymeric foam [9], and paper [10]; roughness of fracture fronts in peeling experiments with PDMS samples [11–13]; and precursor events in the catastrophic collapse of cliffs [14], landslides [15] etc. In particular, it considers a set of elements having finite failure thresholds drawn from a probability distribution as a simple model for a disordered solid. Evolving this model requires a rule of transferring the load between elements, following the breaking of one such element. Given that the width of the distribution function from which the strength of the elements are drawn is finite, the universal macroscopic responses are determined by the range of this load redistribution [16]. The local (nearest neighbors, introduced in [17]) and mean-field (global load sharing [16]) limits are well studied but are rather idealized in view of the fact that any realistic stress concentration range in a solid is neither of these two extremes. Several attempts have been made to interpolate between these two limits [18–22]. However, in the case of catastrophic failures, the stress at which the system just breaks (critical stress) becomes non-zero only when the range of interaction is sufficiently large, so that it suppresses any spatial stress concentration [22]. Hence, statistics that are qualitatively similar to experiments [23] are observed only in the mean-field limit.

The above case of a fiber bundle model with system-wide loading can be contrasted with the case of a model where a load can be applied locally [24], for example at some internal point, or along an edge or interface. In such cases fibers will break around the source of the load, and will then transfer their burden to other nearby fibers. A

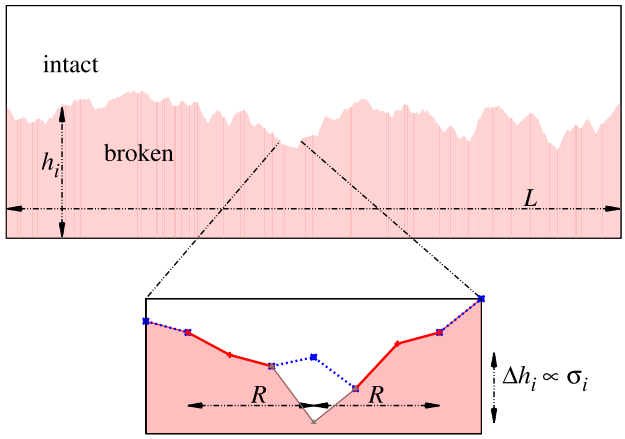

Figure 1. A snapshot of the interface between the broken (red) and unbroken (white) parts of the model system is shown. A magnified portion of the interface demonstrates the breaking of an element along the fracture front (dotted line) and the subsequent advancement of the front. The load of the broken fiber is redistributed to $R = 3$ neighbors (shown in red).

dynamic interface will then develop between the growing region of failed fibers, and the unbroken fibers further from the load. Essentially, this interface will now behave as the tip, or edge, of a growing crack. In a simpler version of this model, which we will develop here, one can simply keep track of the fibers along this effectively one-dimensional interface, at any given time (see figure 1). The stress concentration and dynamics of this model are, therefore, constrained to an activity front that separates two distinct sides: on one side of this front all the material is broken and on the other side it is completely intact. Such confinement of activity can also be achieved with system-wide loading in a two dimensional model, and a gradient in the failure thresholds of the fibers [20] in the direction perpendicular to the desired front. Indeed, two regimes of front roughness were recently found in such a case [21], one consistent with the elastic line and the other coalescence dominated regime.

The activity front, or the failure interface, can be driven through the system quasi-statically, giving rise to intermittent dynamics. The phase transition associated with these intermittent dynamics is the depinning transition of the interface (see e.g. [11, 25]). The states to either side of the corresponding critical point lie in the depinned phase, where the interface moves with a finite steady state velocity, and the pinned phase, where the interface is stopped by pinning centers (see e.g. [12]). This situation is widely observed in different physical systems, for example the vortex lines in superconductors [26], domain walls in magnetic systems [25], charge density waves [27], contact line dynamics in wetting [28] and, of course, in mode-I crack opening [29], on which we shall focus.

Unlike the case of catastrophic failure, in the interface depinning model even the extreme case of a nearest neighbor interaction will have a finite critical load at which the interface depins. It therefore gives a chance to study the effect of spatial fluctuations on interface dynamics. Previous studies regarding interface propagation in fiber bundles include simulations where the fibers were fixed between a rigid ceiling and a soft bottom plate [30]. For a single point loading and redistribution along the interface, the damaged region grew radially outwards on average, resulting in a continuously growing interface [24]. The interface length was proportional to the applied load, resulting in a steady value of the load per fiber along the interface. The intermittent dynamics of the interface showed scale-free statistics.

In our work, a systematic study of the roughness and avalanche dynamics of the fiber bundle model is made by varying the range of interaction along a propagating interface. In particular, we approximate this interface by a one-dimensional array of fibers, and then consider the implications of different types of load redistribution between these interfacial fibers, when one breaks. First, we consider the case of a uniform redistribution over a finite range that can vary from the nearest neighbors of the broken fibers, to the entire interface (i.e. equivalent to a mean-field model). This can include many different types of interaction that have a finite interaction range, for example those due to geometric effects like confinement to a thin sheet, plastic deformation, finite agglomerate size, etc. In such systems we demonstrate a crossover value of the range of interaction of the load redistribution that separates the local and mean-field behaviors. Secondly, we consider a scale-free interaction, where the load from a broken fiber is shared amongst all the fibers along the interface, in an amount inversely proportional to the distance of the fibers from the broken one, raised to some power. Among the scale-free interaction ranges, the inverse-square interaction has been considered before [31], inspired by the stress concentration field around a crack in an infinite sample. The inverse square interaction, however, is not guaranteed for a finite sample [32, 33], which is often a realistic scenario. For example in the fracture or debonding of a paint film, or other thin

coating, the stress is redistributed over a distance comparable to the film thickness [34]. Also the range of the interaction in a real material sample can be affected by the correlation length of any disorder (see e.g. [35]), the size of any aggregates or agglomerates in ceramics [36] or the size of a plastic or process zone in a ductile metal [37, 38], for example. We find that the inverse square interaction lies in the middle of a continuously changing set of critical exponents for the roughness and avalanche size distributions. For very slow decay of the interaction strength with distance, the model is mean-field-like, but it starts deviating from mean-field behavior as soon as the average range of the interaction is finite.

In the following, we first describe our model and then present the numerical results obtained from it. We give analytical calculations for the nearest-neighbor interaction and show that this case is qualitatively different from an elastic interface model approach in that limit. Finally, we make comparison with mode-I crack propagation experiments and offer some conclusions about the effect of finite range interactions on fracture problems.

2. Model

We model the crack front of a mode-I fracture by a line of breakable fibers, as sketched in figure 1. Essentially, we store the stress profile and the position of the front in a one-dimensional array, which is periodically updated. Note that in this way we can work with a one-dimensional model of a front, which is propagating on a hypothetical two-dimensional plane. When the stress on an element exceeds its failure threshold, drawn randomly from a uniform distribution in $[0:1]$, there is a local failure and the front at that point is advanced by an amount proportional to the stress at that point prior to the failure. Hence, while the locations of the fibers are regular and discrete along the front, they are continuous along the propagation direction. After a fiber is advanced, the stress on it is set to zero. The stress that it had carried is partly dissipated (a fraction δ) and the remaining part (the fraction $1-\delta$) is redistributed along the rest of the fracture front, as detailed below. Throughout this paper we have used $\delta = 0.0001$ to study intermittent dynamics, and $\delta = 0$ to study the effects of sudden, fixed loading. For finite δ, our results were found not to depend on the specific value of δ, unless it was larger than about 0.01.

By construction the fracture front can only move forward, hence no islands or overhangs are allowed along the front. The total displacement of the ith element, $h_i(t)$, upto time t is proportional to $\sum_{t\in\mathcal{T}_f}\sigma_i(t)$, where $\sigma_i(t)$ is the instantaneous stress at position i and $\mathcal{T}_f$ is the set of all the times where a fiber failed at that location. Note that the proportionality constant has no effect on the macroscopic measures studied here. The dynamics of the front, except for the stress redistribution rule, are those followed in [31].

In terms of loading our system, we will consider two loading scenarios. First, to establish a simple point of comparison with mean-field models, a fixed load is suddenly applied to the entire system at once. Following failure this load is then redistributed without dissipation. In contrast, for the case of quasi-static loading, on which we focus, the external force increases slowly with time, like the case of peeling a piece of tape off a table. This increase in load can cause fibers to break, and thereby advance the fracture front. However, in any real experiment there must be a finite dissipation of stress as the front advances. This can be due to acoustic emissions, friction, heat, etc or simply the finite compliance of any load cell. The dissipation will halt any advance, but the increase in load will then continue until another advance happens, and so on. These two competing mechanisms, loading and dissipation, lead to intermittent dynamics of the front. In our simulations we capture this by alternating between slow loading steps and fast front activity, including dissipation. Now the load is increased until the first fiber breaks, then it is stopped and the load redistribution rules are followed until the avalanche of activity stops, on the assumption that internal load redistribution occurs much faster than the recovery of the external loading. When dissipation stops the avalanche, further loading is continued. In this way any system will self-organize, tending towards the critical point of the depinning transition in the corresponding conservative system (figure 2). To avoid observing transient behavior, the first 10 000 to 100 000 avalanches (depending on the system size) were excluded from analysis.

We will also explore two types of redistribution rules, following the breaking of a fiber. First, we will consider the case where the redistribution only affects fibers within a finite range, which can be as small so as to include only the nearest neighbors, or as large as the system size. For this we consider the uniform redistribution of the load to R neighbors on each side of the failed fiber, along the interface (i.e. affecting a total of $2R$ fibers). Redistributions that affect a finite range are expected to be captured by this process, which is also the case for catastrophic failure [22]. The two extreme cases are the nearest neighbor ($R = 1$) and mean-field ($R \sim L$, where L is the system size) interactions and we find a crossover length scale R_c above which the system starts behaving like the mean-field limit.

Secondly, we will consider scale-free redistribution, i.e. if the fiber at the ith site fails then a fiber at the jth site will receive a load proportional to $1/|i-j|^{\gamma}$. Here, for small enough values of γ, and hence more long-range

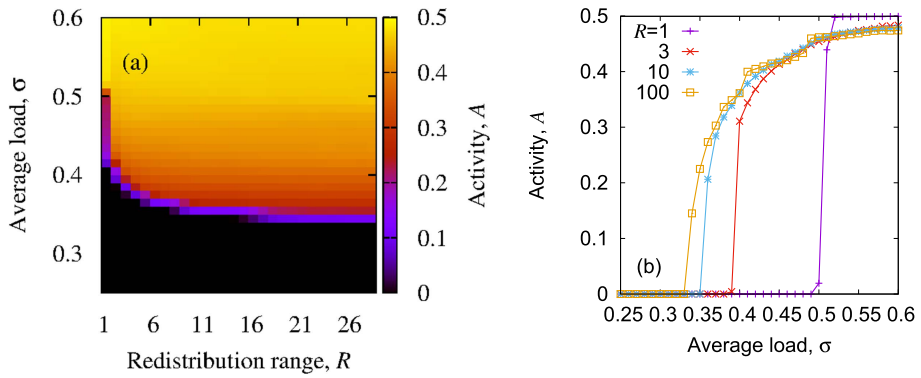

Figure 2. (a) The phase diagram for the depinning transition with a range dependent load transfer. The color scale gives the steady-state breaking rate or activity, A, for simulations run at different loads σ and ranges R. As can be seen, the nearest neighbor case $R = 1$ shows a sharp jump in the activity at the critical point $\sigma = 0.5$. In the presence of dissipation ($\delta > 0$), and for a slow quasi-static drive, the critical point becomes an attractive fixed point, causing the load per fiber to saturate at its critical value. (b) Activity rates for various values of R show how its discontinuous jump for $R = 1$ gradually disappears as R becomes large. The system size is $L = 1000$.

coupling, the interaction is expected to be mean-field. For sharp enough decay (large γ values) the behavior will be local. Once again, a crossover $\gamma_c = 1$ is found above which the behavior of the activity front starts deviating from the mean-field limit. The system also then shows a continuous variation in its critical exponent values for roughness and avalanche size, until it reaches the other limit, a nearest neighbor interaction, for large enough γ.

3. Results

We report on the effects of two types and redistribution rules here, following the breaking of a fiber. These involve either the redistribution of the load evenly over a finite range (sections 3.1 and 3.2), or a scale-free redistribution that decays with some characteristic power-law (section 3.3). For the finite-range redistribution, the case without dissipation (section 3.1) is considered separately from the quasi-static case (section 3.2).

3.1. Depinning transition with non-dissipative finite range interaction

Let us first look into the case where the load redistribution is of finite range. Following a failure, the load is redistributed to $2R$ nearby fibers, without dissipation. The fracture front propagating through the system shows a depinning transition [39] when sufficient load is applied. This depinning transition is seen in the limit of no dissipation ($\delta = 0$) or, in practice, when dissipation is negligibly small as compared to the total load ($\delta \ll 1$). It is an active-absorbing kind of phase transition [40]. The order parameter is defined here as the rate of activity, A, or the number of fibers breaking per Monte Carlo time-step. For a large enough load it reaches a stationary non-zero value (active state), on average. When the load per fiber is below some critical value σ_c, it falls to zero (absorbing state). Figure 2(a) shows the phase boundary between these active and absorbing states for different values of the interaction range, R. The color (shade) gradient gives the activity rate A. The $R = 1$ case shows a sharp jump (see figure 2(b)), suggesting a discontinuous transition there.

We will now look more carefully into the critical behavior for the nearest neighbor ($R = 1$) case without dissipation. Consider the situation where a load σ, per fiber, is applied uniformly and suddenly on the system. All fibers with a failure threshold below σ will break. This will create broken patches, the largest of which is most likely to contribute to further breaking the system, leading to depinning. If all the stress from this patch, of length l, is redistributed to the two neighboring points on either side of the patch, these points will now each carry a load $\sigma + \frac{\sigma l}{2}$. Since l is large, this will likely cause further breaking and in the next time step the increased stress at the edge of the growing active region will be $\sigma + \frac{1}{2}\left(\sigma + \frac{l\sigma}{2}\right)$. After m such steps, the load on the sides of the patch will be

$$\begin{aligned} \sigma_E &= \left(\sigma + \frac{\sigma}{2} + \frac{\sigma}{4} + \ldots + \frac{\sigma}{2^m}\right) + \frac{l\sigma}{2^m} \\ &= 2\sigma + \frac{\sigma(l-1)}{2^m}. \end{aligned} \tag{1}$$

The second term is an exponential decay, which vanishes for large m. The first term will cause depinning i.e. breaking all possible pinning centers, only when the stress exceeds the maximum pinning threshold 1, giving a

critical load $\sigma_c = 1/2$. The above calculation is valid in the sub-critical limit, where large m values are possible, and therefore gives the limiting stress that the system can withstand without depinning. This is the critical load that we see in the simulations as well (see e.g. figure 2 for $R = 1$). Also, at the critical load $1/2$, it is trivially seen that half of the system on average will break in the first time step following the loading. After redistribution of this load, the surviving fibers will have stress 1 on average and will then break in the following time step. These two steps will continue to repeat in the steady state, giving an average activity rate of $1/2$. Note that this is a discontinuous jump from zero activity in the absorbing phase (for $\sigma < \sigma_c$). This is in contrast to the nearest neighbor elastic line (Edwards–Wilkinson model [41]) depinning, which shows a continuous transition [42] instead.

The other extreme case, for a response to a sudden loading, is the continuous depinning transition in the mean-field limit ($R \sim L$). Unsurprisingly, the mean-field exponents are recovered there (see appendix).

3.2. Intermittent dynamics with dissipative finite range interaction

Let us now explore the critical response to quasi-static loading in the presence of dissipation. After an initial failure the load is redistributed, as described in section 2, and a fraction of the load from each failing fiber is dissipated. The dissipation implies that the front propagation will eventually halt, at which point we resume increasing the load, slowly, to restart the dynamics.

We will study the dynamic (avalanche statistics) and static (roughness of the front) properties of the dissipative system for different load redistribution rules, including the local and mean-field limits, and intermediate conditions. We aim to understand the crossover dynamics between the two very different end-members of this model, and to determine the redistribution range at which the model behavior shifts from local to mean-field.

3.2.1. Avalanche statistics

The total number of fibers breaking between two successive loading steps, denoted by S, measures the size of an avalanche. The number of load redistribution steps before the avalanche stops is the duration of the avalanche T. In figure 3 the size distribution, $P(S)$, and duration distribution, $Q(T)$, of the avalanches are plotted for different values of R. Both distributions show a crossover in the exponent value of a power-law fit, beyond a given size (or duration), and the crossover size (duration) increases with increasing R. While a precise crossover scale will be obtained later (section 3.2.3), from these plots it is intuitively clear that for a given R small avalanches will not see the scale of load redistribution and will give mean-field statistics, since the load distribution within that range is uniform. Only the larger avalanches, involving several redistribution steps, will feel the effect of the load redistribution range and hence deviate from mean-field behavior.

3.2.2. Roughness exponent of the front

The response of the system in the vicinity of the depinning critical point can be studied from its dynamics, as done above, and also from its static characteristics, for example in the roughness of the propagating front. The self-similar nature of the front, at any given moment, in the case of fracture is well studied (see [39] for a review). In order to demonstrate the roughness properties of our model, we measure the amplitude of the height fluctuations

$$C(r) = \langle (h_{i+r} - h_i)^2 \rangle^{1/2} \sim r^{\zeta_r}, \tag{2}$$

where the angular brackets give the average over space and ζ_r is the roughness or Hurst exponent. This exponent can also be estimated in Fourier space [43], via the decay of the power spectrum of h,

$$\langle |\tilde{h}(k)|^2 \rangle \sim k^{-1-2\zeta_k}, \tag{3}$$

where ζ_k is another measure for the roughness exponent. Both the auto-correlation and power-spectral methods attempt to describe the same thing, namely the scaling exponent of a self-affine curve. Usually they are equivalent, except in certain limits, such as the case of very small (or even negative) roughness exponents [44, 45]. Here we will focus on the more common, real-space measurement. However, in section 3.3, when small or negative exponents are expected, we will compare the two methods.

Following the measure defined in equation (2), figure 4(a) depicts the behavior of the roughness as the interaction range R is varied. As in the case of avalanche statistics, the scaling functions also show a crossover in critical exponent, depending on the value of R. Clearly, as long as $r < R$, $C(r)$ should be independent of r, since there is no notion of spatial distance within that range. In other words, over distances shorter than the interaction length R, the system should appear as mean-field-like. It is only when we look for correlations over large enough length scales (i.e. bigger than R), that anything else would be expected. In particular, for $r > R$, we find a non-trivial scaling exponent, with $\zeta_r \simeq 0.9$. This point is further clarified in figure 4(b), where the distance r is normalized by R. All curves then show the same crossover in roughness near the point $r \approx R$.

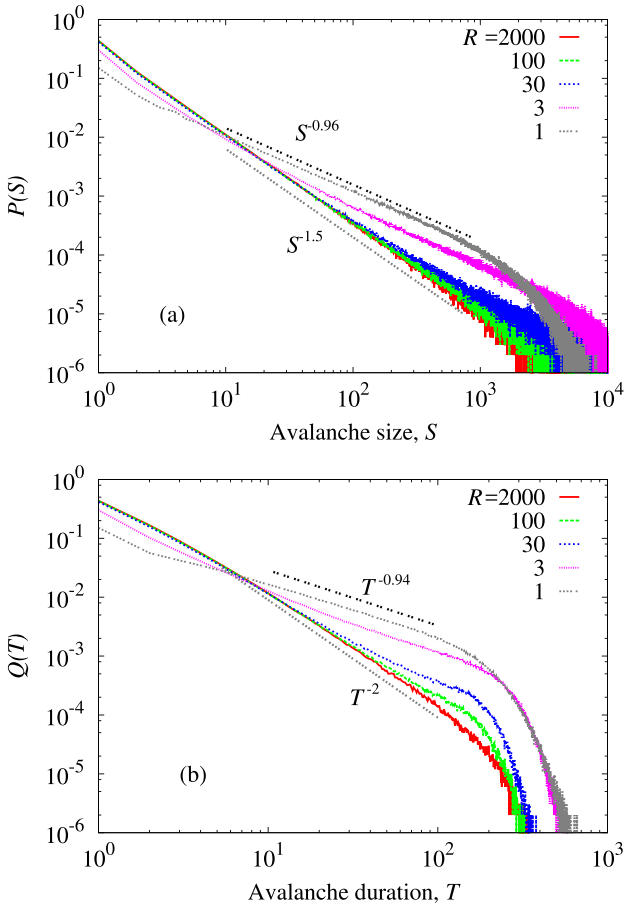

Figure 3. The size (a) and duration (b) distributions of avalanches are shown for different values of R and a system size $L = 10\,000$. A crossover in the exponent values for size (duration) is seen from a mean-field value of 1.5 (2) to a local value of 0.96 (0.94). The latter scaling exponents are best-fit values to the numerical results at $R = 1$. As discussed in the text, smaller avalanches do not see the load sharing range R, hence follow mean-field statistics.

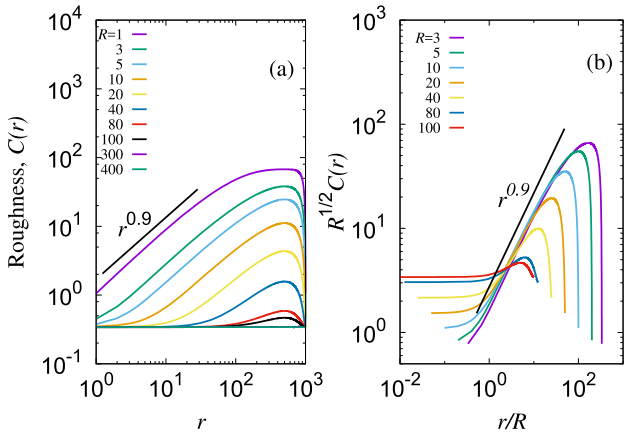

Figure 4. (a) The self-similar scaling of the roughness of the front is shown, following the measure given in equation (2). The height fluctuations in the mean-field limit ($r/R \to 0$) show no variation with r, since there is no notion of distance below the length scale R. (b) When distance is scaled by R, all crossover points collapse to the same value, as does the scaling of the roughness both above and below the point $r = R$. The system size is $L = 1000$.

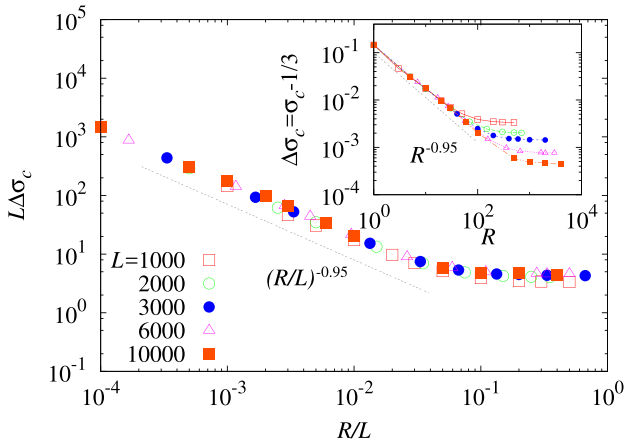

Figure 5. The inset shows how the critical load approaches the mean-field limit as R increases. Beyond some crossover value R_c, the quantity $\Delta\sigma_c$ becomes independent of R, signaling the change from local to mean-field behavior. The main panel shows how all data collapse when scaled by system size, confirming that $R_c \sim L$. In other words, when the interaction range R is larger than roughly 10% of the system size, the system behaves like the mean-field case.

3.2.3. Crossover scale

For a more precise measure of the crossover scale, we look at the long time average of the load per fiber (which is also the critical stress σ_c) on the system for different values of R. In the mean-field limit, the stress is expected to saturate to $1/3$, as was the case in [24]. We therefore look at the quantity $\Delta\sigma_c = \sigma_c(R, L) - 1/3$, which will tend to zero as either the interaction range R or the system size L is increased. For a given system size, however, finite size effects will make $\Delta\sigma_c$ saturate at a small but finite value. A crossover scale, consistent with our usage in section 3.2.2, can be defined from the point where $\Delta\sigma_c$ starts becoming independent of R. Quantities behaving independently of R are the signature of the mean-field limit.

In figure 5 the dependence of $\Delta\sigma_c$ on the redistribution range R for different system sizes is plotted. The inset shows how the crossover behavior depends on the system size, and also demonstrates how $\Delta\sigma_c$ decreases to zero as the system size grows. Data collapse is obtained by scaling the distance with L. This implies that $R_c \sim L$, or that a significant fraction of the system must be covered by the load sharing range in order for the system to show mean-field like behavior.

3.3. Intermittent dynamics with dissipative scale-free interactions

Finally, we study the effects of varying the load redistribution process. Now, following a failure at site i, the load received at site j will be proportional to $\rho = \frac{1}{|i-j|^\gamma}$. As one example of such a response, linear-elastic theory predicts an inverse square ($\gamma = 2$) [46, 47] load redistribution for an infinite sample. However, the redistribution range and scaling behavior can be modified due to effects such as a finite sample [32, 33], the width of the sample [34], any correlation in the local disorder [35], and so on. In such situations, a scale free load redistribution is closer to what one can expect, instead of the finite range interaction presented in the preceding sections.

The case $\gamma = 2$, which corresponds to a classic Inglis crack, was studied in [31]. But here we show that the $\gamma = 2$ case lies in the middle of a continuously varying 'universality' that interpolates between local and global scenarios. Hence a small change in γ can lead to a significant change in macroscopic observables, such as activity statistics and roughness exponents.

Before summarizing the numerical results, let us briefly look into how the crossover value of the exponent γ may be predicted from the linear scaling of R_c with system size obtained in the previous section. Even for a 'scale-free' distribution there are still two obvious scales: the lower cut-off scale of the interaction range is the lattice spacing and the upper cut-off is the system size. Hence it is possible to define an effective range $R_{\text{eff}} = \int_1^L r\rho(r)\,dr$ with $\rho(r)$ being the (normalized) power-law redistribution of load. It can be shown [22] that $R_{\text{eff}} = \frac{1-\gamma}{2-\gamma}\frac{L^{2-\gamma}-1}{L^{1-\gamma}-1}$. For $1 < \gamma < 2$, $R_{\text{eff}} \sim L^{2-\gamma}$, which must match with $R_c \sim L$ at the crossover point. This gives $2 - \gamma_c = 1$ i.e. $\gamma_c = 1$. So for any value of γ larger than 1, the average redistribution range of the load will be smaller than the system size, and thus mean-field-like behavior can no longer be expected. However, as we shall see, this deviation from the mean-field response does not necessarily imply local load sharing behavior for other measures, such as the avalanche and roughness statistics.

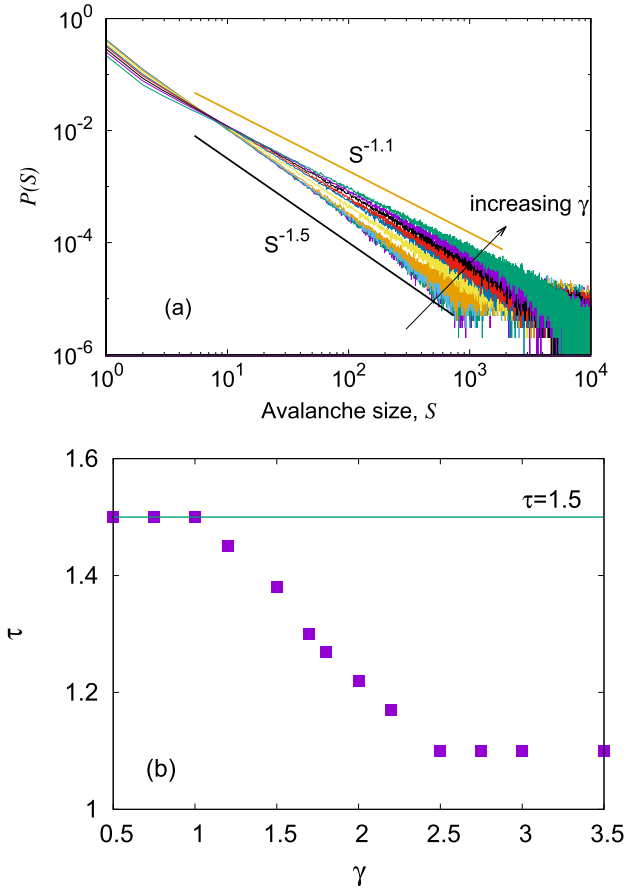

Figure 6. (a) The avalanche size distributions $P(S)$ are plotted for different values of γ. They have the scale invariant form $P(S) \sim S^{-\tau}$. The exponent τ varies with γ as shown in panel (b). As mentioned in the text, the departure from the mean-field exponent 1.5 is seen for $\gamma > \gamma_c = 1$. The system size is $L = 10\,000$.

Note that $\gamma_c = 1$ is also an intuitive result from the fact that for $\gamma \leqslant 1$ the effective range diverges for an infinite system. But that does not exclude the possibility of a mean-field response where $\gamma_c > 1$, which is indeed the case for catastrophic breakdown [22]. Therefore, the above result is a joint consequence of the linear scaling $R_c \sim L$ and the divergence of the effective range for $\gamma \leqslant 1$.

In figure 6(a), the avalanche size distributions are plotted for different γ values. They show a continuous variation in the exponent τ of the size distribution, $P(S) \sim S^{-\tau}$, as detailed in figure 6 (b). As expected, the departure from the mean-field value ($\tau = 1.5$) starts from just above $\gamma_c = 1$.

To measure the roughness exponent, we here use both the real-space (autocorrelation) method of equation (2) and the Fourier-space (power-spectral) method of equation (3). The latter technique is more general, and is capable of measuring negative roughness exponents, such as are expected for example in the case of white noise (where $\zeta_k = -0.5$) [30]. Power law fits are used to find the respective exponents ζ_k and ζ_r for each γ, and these roughness exponents are shown in figure 7. For the similar situation of a fluctuating elastic line, both theory [48] and simulations [43] predict a relation $\zeta_k = (2\gamma - 3)/3$, which is also plotted in the graph. Around $\gamma = 2$ it follows our simulation points well. Away from this intermediate case there is departure from the elastic line simulations, in particular for high γ values. This further underlines the difference between the macroscopic modeling approach of the elastic line and the microscopic discrete model studied here. They differ quantitatively as the interaction range becomes localized (high γ), while keeping the correspondence near the linear-elastic regime at $\gamma = 2$.

4. Discussion and conclusion

The common features that arise in various physical systems such as domain walls in magnetic materials, vortex lines in superconductors, charge density waves, contact line dynamics in wetting and also in mode-I fracture, is that an 'elastic' line or front is driven by an external parameter (a magnetic field, mechanical force, etc) through a

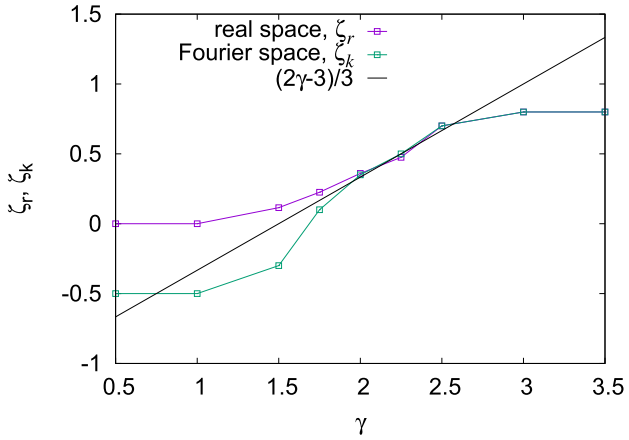

Figure 7. The roughness of the front produced for scale free load redistribution is measured by analyzing the auto-correlation (equation (2)) as well as the power spectrum (equation (3)). The continuous variation of the roughness exponents ζ_r and ζ_k with γ is obtained. Near $\gamma = 2$ they match with the theoretical prediction [43, 48], shown by the straight line, of a fluctuating elastic line. For small values of γ, the negative roughness exponent values are obtained for Fourier space measurements, which can not be seen in the real-space measurements. The system size is $L = 1000$.

medium with many obstacles (impurities, variations in breaking strength, etc). This results in intermittent dynamics of the moving front. The classification of the properties of such a front depends on its elastic nature, or in other words, the range upto which the front is affected following a local perturbation.

Here we have reported the critical properties of such a front through a simple, discrete fiber bundle model approach. The different strengths of the fibers represent the disorder in the material. While this is a generic model for interface propagation in the cases mentioned above, we focused on mode-I fracture front propagation in this study. Assuming the applied load to be localized along a line, we can track the activity of that line. We aimed at determining the influence of a variable range of interaction, characterizing the load redistribution range following the failure of a fiber along the interface, on macroscopic static and dynamic properties of the interface, such as roughness and avalanche statistics. We found such macroscopic observables to be very sensitive to the range of interaction. In particular, we could identify a crossover from local, nearest-neighbor-like behavior to global, mean-field-like behavior by varying the range of load redistribution. We showed how this could be done directly, using a flat distribution over a finite neighborhood, or indirectly by varying the exponent γ in the case of a power-law load redistribution. The crossover range R_c scales linearly with the system size in the case of a finite range redistribution. This situation corresponds to $\gamma_c = 1$, for which the behavior deviates from the mean-field in the case of power-law load redistribution. For a power-law load redistribution, a continuously varying set of exponents are obtained for the avalanche size statistics and the roughness of the front. Interestingly, the $\gamma = 2$ case lies in the middle of such a continuous variation, implying that any change in γ will be reflected in the roughness and avalanche size exponent values.

An obvious point of comparison for these results is with the elastic interface model [49]. This model is formulated from an opposite approach to ours, in the sense that it is a macroscopic model. Models of this type consider the elastic interactions of the interface line from the perspective of linear-elastic fracture mechanics, where the disorder of the material is treated as quenched noise, as opposed to a microscopic modeling of the disordered solid. The elastic interaction can fall off with distance r from a local perturbation as $1/r^{\gamma}$. Similar characterization, by varying the parameter γ, leads to a continuous variation in the roughness exponent value [43], and also crossover behavior [50]. We find the mean-field limit of these two approaches are the same; both in terms of roughness of the interface, which lacks spatial correlation at this point, and also in terms of the avalanche size distribution. Particularly, the roughness exponent approaches -0.5 and the avalanche size distribution exponent becomes 1.5 for both of these models. Also, for $\gamma = 2$, the roughness exponents are close to each other and this also compares well with the result in [21], where the elastic line limit was observed in the large scale limit. But apart from the mean-field limit, or dimensions higher than 4 [51], they are both quantitatively (e.g. figure 7 for higher γ values) and qualitatively different (e.g. for fiber bundles the depinning transition is discontinuous for the nearest neighbor interaction) from the fiber bundle model of an interface.

Many experiments have been done on fracture front propagation in disordered solids in the last couple of decades [5, 6]. Among other things, they concern themselves with the in and out-of-plane roughness properties of broken surfaces, measured both along and perpendicular to the direction of the crack front [39]. The situation is somewhat simplified when out of plane roughness is suppressed and the crack propagates along an easy plane

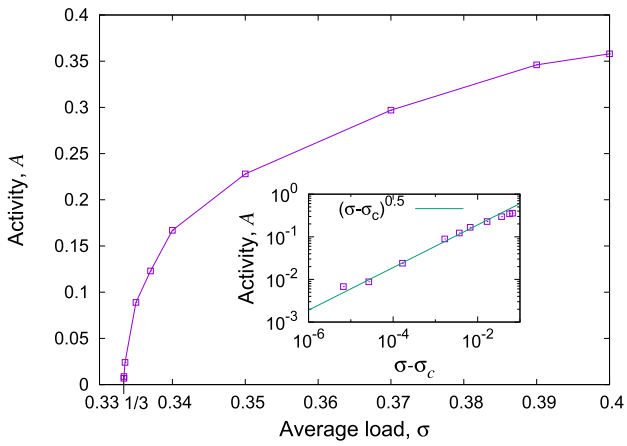

Figure A1. The growth of the order parameter A beyond the critical load σ_c is shown. The inset shows the power-law fitting with an order parameter exponent value $\theta = 1/2$. The system size is $L = 700\,000$.

only, resembling the in-plane motion of the front studied here. Particularly, in [11] two Plexiglas plates were sandblasted, joined together and then slowly forced open from one edge such that a mode-I crack opening took place. The propagating front was viewed by the loss of transparency of the joined plates. The avalanche dynamics and roughness properties of such fronts are well studied [12, 13, 52, 53]. Apart from showing a crossover in response from small-to-large length scales, the roughness exponent measurements also show differences in these two limiting regions. The avalanche exponent can be significantly lower (1.1) than predicted (1.28) by the elastic interface model with inverse square elastic strength [33], but also there exists a large spread in the measured values of such exponents in different experiments [23]. Such a spread is not unique to the case of fracture front propagation, but is also seen in the cases of domain wall dynamics in magnetic systems [54–56], and fluid invasion fronts in porous media [57]. Although several mechanisms were proposed to explain these differences, such as driving rate, correlation in disorder, microscale coalescence and so on, no consensus has yet been reached. Our simulation shows how one can relate such a change in exponent values with the variation of an effective interaction range, which in turn can be due to one or more of the reasons mentioned above.

In conclusion, the interface propagation in the fiber bundle model shows a crossover behavior from local to mean-field statistics as the range of the interaction is increased. The crossover length scales linearly with the system size. This implies that for power-law load sharing with exponent values greater than one, the behavior will be different from the mean-field. This simple prediction is also confirmed numerically. A continuous variation in the avalanche size and roughness scaling exponent values were seen with different powers of the scale-free load sharing, making it a very relevant parameter to keep in mind while considering the finite scales of interaction that might arise in experimental situations.

Appendix. Depinning transition exponents in the mean field limit

When $R \sim L$, the depinning transition seen in our model is the mean-field type. The growth of the order parameter, here the activity rate, above the critical load behaves as $A \sim (\sigma - \sigma_c)^{\theta}$. Assuming the scaling form

$$A(t) \sim t^{-\alpha} F(t^{1/\nu}|\sigma - \sigma_c|,\ t^z/L), \tag{A.1}$$

we can estimate the scaling exponents α, ν and z and also verify the scaling relation $\alpha = \theta/\nu$, in this limit.

In figure A1 we plot the saturation activity rates at different σ values above $\sigma_c = 1/3$ for the mean-field case of $R = L$. The inset shows the power-law variation $(\sigma - \sigma_c)^{1/2}$, giving $\theta = 1/2$, which matches with the prediction for the mean-field elastic interface [58]. At the critical point the order parameter decays as $A(t) \sim t^{-\alpha}$, where t is the time measured by the number of load redistribution steps. This is seen in figure A2, with $\alpha \approx 0.5$. Also, by plotting $A(t)t^{\alpha}$ with $t|\sigma_c - \sigma|^{\nu}$ and by tuning ν, we get a data collapse near $\nu \approx 1.0$ (see figure A2). This agrees with the scaling relation $\alpha = \beta/\nu$. Finally, for the finite size scaling at the critical point, the cut-off time scale τ scales with system size as $\tau \sim L^{1/z}$ with $z \approx 2.0$. This set of exponents defines the mean-field depinning transition for fiber bundle interfaces, and these results show that our model reaches this well-defined response in the appropriate limit.

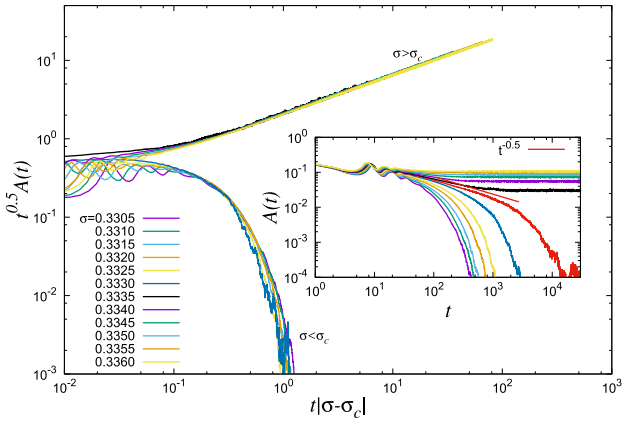

Figure A2. The super-critical and sub-critical behavior of the order parameter with time are shown. At the critical point a power-law decay gives the exponent $\alpha \approx 0.5$ and the off-critical collapse shows gives the scaling exponent $\nu = 1.0$. The system size is $L = 100\,000$.

References

[1] Peirce F T 1926 *J. Text. Inst.* **17** T355
[2] Daniels H E 1945 *Proc. R. Soc.* A **183** 405
[3] Phoenix S L and Taylor H M 1973 *Adv. Appl. Probab.* **5** 200
[4] Chakrabarti B K and Benguigui L G 1997 *Statistical Physics of Fracture and Breakdown in Disordered Systems* (Oxford: Oxford University Press)
[5] Sahimi M 2003 *Heterogeneous Materials II: Nonlinear and Breakdown Properties* (New York: Springer)
[6] Biswas S, Ray P and Chakrabarti B K 2015 *Statistical Physics of Fracture, Breakdown and Earthquake* (New York: Wiley)
[7] Garcimartin A, Guarino A, Bellon L and Ciliberto S 1997 *Phys. Rev. Lett.* **79** 3202
[8] Guarino A, Garcimartin A and Ciliberto S 1998 *Eur. Phys. J.* B **6** 13
[9] Deschanel S, Vanel L, Vigier G, Godin N and Ciliberto S 2006 *Int. J. Fract.* **1** 87
[10] Salminen L I, Tolvanen A I and Alava M J 2002 *Phys. Rev. Lett.* **89** 185503
[11] Schmittbuhl J and Måløy K 1997 *Phys. Rev. Lett.* **78** 3888
[12] Santucci S, Grob M, Toussaint R, Schmittbuhl J, Hansen A and Måløy K J 2010 *Europhys. Lett.* **92** 44001
[13] Chopin J, Boudaoud A and Adda-Bedia M 2015 *J. Mech. Phys. Solids* **74** 38
[14] Amitrano D, Grasso J R and Senfaute G 2005 *Geophys. Res. Lett.* **32** L08314
[15] Cohen D, Lehmann P and Or D 2009 *Water Resour. Res.* **45** W10436
[16] Pradhan S, Hansen A and Chakrabarti B K 2010 *Rev. Mod. Phys.* **82** 499
[17] Harlow D G and Pheonix S L 1978 *J. Compos. Mater.* **12** 195
[18] Hidalgo R C, Moreno Y, Kun F and Herrmann H J 2002 *Phys. Rev.* E **65** 046148
[19] Pradhan S, Chakrabarti B K and Hansen A 2005 *Phys. Rev.* E **71** 036149
[20] Stormo A, Gjerden K S and Hansen A 2012 *Phys. Rev.* E **86** 025101(R)
[21] Gjerden K S, Stormo A and Hansen A 2013 *Phys. Rev. Lett.* **111** 135502
[22] Biswas S, Roy S and Ray P 2015 *Phys. Rev.* E **91** 050105(R)
[23] Bonamy D 2009 *J. Appl. Phys.* D **42** 214014
[24] Biswas S and Chakrabarti B K 2013 *Phys. Rev.* E **88** 042112
[25] Zapperi S, Cizeau P, Durin G and Stanley H E 1998 *Phys. Rev.* B **58** 6353
[26] Larkin A I and Ovchinnikov Y N 1979 *J. Low Temp. Phys.* **34** 409
[27] Fisher D S 1985 *Phys. Rev* B **31** 1396
[28] Chevalier T and Talon L 2015 *Eur. Phys. J.* B **38** 76
[29] Bouchaud J P, Bouchaud E, Lapasset G and Planes J 1993 *Phys. Rev. Lett.* **71** 2240
[30] Batrouni G G, Hansen A and Schmittbuhl J 2002 *Phys. Rev.* E **65** 036126
[31] Pontuale G, Colaiori F and Petri A 2013 *Europhys. Lett.* **101** 16005
[32] Hutchinson J W and Suo Z 1991 *Adv. Appl. Mech.* **29** 63
[33] Barés J, Hattali M L, Dalmas D and Bonamy D 2014 *Phys. Rev. Lett.* **113** 264301
[34] Xia Z C and Hutchinson J W 2000 *J. Mech. Phys. Solids* **48** 1107
[35] Peng C, Havlin S, Schwartz M and Stanley H E 1991 *Phys. Rev. Lett.* **44** R2239
[36] Kendall K, Alford N McN, Clegg W J and Birchall J D 1989 *Nature* **339** 130
[37] Barenblatt G I 1959 *J. Appl. Mech. Solids* **23** 434
[38] Dugdale D S 1960 *J. Mech. Phys. Solids* **8** 100
[39] Bonamy D and Bouchaud E 2011 *Phys. Rep.* **498** 1
[40] Henkel M, Hinrichsen H and Lübek S 2014 *Non-Equilibrium Phase Transitions* (Berlin: Springer)
[41] Edwards S and Wilkinson D 1982 *Proc. R. Soc.* A **381** 17
[42] Amaral L, Barabási A, Makse H and Stanley H E 1995 *Phys. Rev.* E **52** 4087
[43] Tanguy A, Gounelle M and Roux S 1998 *Phys. Rev.* E **58** 1577
[44] Hansen A, Schmittbuhl J and Batrouni G G 2001 *Phys. Rev.* E **63** 062102
[45] Yang H-N and Lu T-M 1995 *Phys. Rev.* B **51** 2479
[46] Schmittbuhl J, Roux S, Vilotte J-P and Måløy K J 1995 *Phys. Rev. Lett.* **74** 1787

[47] Ramanathan S, Ertas D and Fisher D S 1997 *Phys. Rev. Lett.* **79** 873
[48] Narayan O and Fisher D S 1993 *Phys. Rev.* B **48** 7030
[49] Rice J R 1985 *J. Appl. Mech.* **52** 571
[50] Chen Y J, Zapperi S and Sethna J P 2015 *Phys. Rev.* E **92** 022146
[51] Le Doussal P and Wiese K J 2009 *Phys. Rev.* E **79** 051106
[52] Måløy K and Schmittbuhl J 2001 *Phys. Rev. Lett.* **87** 105502
[53] Måløy K, Santucci S, Schmittbuhl J and Toussaint R 2006 *Phys. Rev. Lett.* **96** 045501
[54] Zapperi S, Cizeau P, Durin G and Stanley H E 1998 *Phys. Rev.* B **58** 6353
[55] Alessandro B, Beatrice C, Bertotto G and Montorsi A 1990 *J. Appl. Phys.* **68** 2901
Alessandro B, Beatrice C, Bertotto G and Montorsi A 1990 *J. Appl. Phys.* **68** 2908
[56] Kim D, Choe S and Shin S 2003 *Phys. Rev. Lett.* **90** 087203
[57] He S, Kahanda G and Wong P 1992 *Phys. Rev. Lett.* **69** 3731
[58] Vannimenus J and Derrida B 2001 *J. Stat. Phys.* **105** 1